
How Do Recommendation Models Amplify Popularity Bias? An Analysis from the Spectral Perspective

Siyi Lin

Zhejiang University
Hangzhou China
lin452_lsy@zju.edu.cn

Chongming Gao

USTC
Hefei China
chongming.gao@gmail.com

Jiawei Chen

Zhejiang University
Hangzhou China
sleepyhunt@zju.edu.cn

Sheng Zhou

Zhejiang University
Hangzhou China
zhousheng_zju@zju.edu.cn

Binbin Hu

Ant Group
Hangzhou China
bin.hbb@antfin.com

Chun Chen

Zhejiang University
Hangzhou China
chenc@zju.edu.cn

Can Wang

Zhejiang University
Hangzhou China
wcan@zju.edu.cn

Abstract

Recommendation Systems (RS) are often plagued by popularity bias. When training a recommendation model on a typically long-tailed dataset, the model tends to not only inherit this bias but often exacerbate it, resulting in over-representation of popular items in the recommendation lists. This study conducts comprehensive empirical and theoretical analyses to expose the root causes of this phenomenon, yielding two core insights: 1) Item popularity is memorized in the principal spectrum of the score matrix predicted by the recommendation model; 2) The *dimension collapse* phenomenon amplifies the relative prominence of the principal spectrum, thereby intensifying the popularity bias.

Building on these insights, we propose a novel debiasing strategy that leverages a *spectral norm regularizer* to penalize the magnitude of the principal singular value. We have developed an efficient algorithm to expedite the calculation of the spectral norm by exploiting the spectral property of the score matrix. Extensive experiments across seven real-world datasets and three testing paradigms have been conducted to validate the superiority of the proposed method.

1 Introduction

Recommender Systems (RS), with their capability to offer personalized suggestions, have found applications across various domains [18, 44, 72]. Nevertheless, their effectiveness in personalization is significantly compromised by popularity bias [12]. This bias emerges when recommendation data showcases a long-tailed distribution of item interaction frequencies. Subsequently, recommendation models trained on such data tend to inherit and even amplify this bias, leading to an overwhelming presence of popular items in recommendation results [56, 68, 74]. This notorious effect not only undermines the accuracy and fairness of recommendation [5, 4], but also exacerbates the Matthew Effect and the filter bubble through the user-system feedback loop [37, 23, 22].

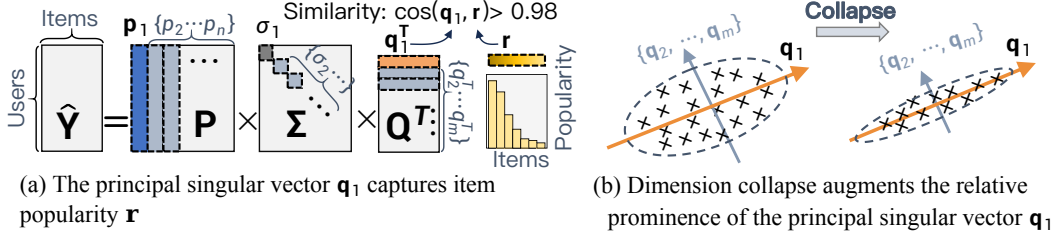


Figure 1: Illustration of two core insights.

Given the detrimental impact of popularity bias amplification, a thorough understanding of its root causes is crucial. Although some recent studies have endeavored to elucidate this, their investigations exhibit significant limitations: 1) Some researchers [56, 68, 55] have investigated popularity bias amplification through causal graphs. However, they merely postulate causal relations between item popularity and model predictions without deeply exploring the underlying mechanisms behind the relations. Moreover, their analyses depend on hypothesized causal graphs, which may be flawed due to the widespread presence of unmeasured confounders [21, 67]. 2) Other studies [73, 69, 11, 65] revealed that graph neural networks (GNNs) can exacerbate popularity bias. However, these analyses are limited to GNNs as applied in specific graph-based recommendation models, rather than the mechanisms of generic recommendation models.

To bridge this research gap, we undertake extensive theoretical and empirical studies on popularity bias amplification. By investigating the spectrum of the ranking score matrix over all users and items predicted by recommendation models, we present the following insights:

1) Memorization Effect. When training a recommendation model on long-tailed data, *the information of item popularity is memorized in the principal spectrum (Figure 1(a))*. Empirically, we observe that the principal singular vector of the score matrix closely aligns with item popularity, with a cosine similarity consistently exceeding 0.98 across multiple representative recommendation models and datasets. Theoretically, we derive the lower bound of this cosine similarity, demonstrating that the similarity converges to one for highly long-tailed training datasets.

2) Amplification Effect. *The phenomenon known as dimension collapse augments the relative prominence of the principal spectrum that captures item popularity, leading to bias amplification (Figure 1(b))*. We reveal that dimension collapse is pervasive in RS due to two primary reasons: i) The deliberate low-rank setting of user/item embeddings, employed either to conserve memory or to counteract overfitting, amplifies the impact of the principal spectrum; ii) The inherent training dynamics of gradient-based optimization prioritize the learning of the principal dimension, while the singular values of other dimensions are easily underestimated. Our further theoretical and empirical analyses establish the relationship between dimension collapse and popularity bias — larger principal singular values compared to other singular values lead to more popular items on the recommendations.

Our analysis not only explains the underlying mechanisms of bias amplification but also paves the way for the development of an innovative strategy to counteract this effect. Recognizing that the essence of this amplification lies in the undue contribution of the principal spectrum, we introduce a spectral norm regularizer [60] aimed at directly restraining the magnitude of the principal singular value. However, the direct computation of the spectral norm necessitates exhaustive processing of a large score matrix and numerous iterative procedures [60, 52], inducing significant computational costs. To address this challenge, we further develop an accelerated strategy by leveraging the intrinsic spectrum properties of the score matrix and matrix transformation techniques. Consequently, our method effectively mitigates popularity bias while imposing limited computational overhead. It is worth noting that our method is model-agnostic and can be easily integrated into various recommendation models. We conduct extensive experiments on seven real-world datasets with three representative backbones, validating the superiority of our proposed method over existing debiasing methods.

2 Preliminaries

Task Formulation. This work mainly focus on the collaborative filtering (CF) [58], a widely-used recommendation scenario. Consider a RS with a user set \mathcal{U} and an item set \mathcal{I} . Let n and m denote the total number of users and items. Historical interactions can be expressed by a matrix $\mathbf{Y} \in \{0, 1\}^{n \times m}$,

where the element y_{ui} indicates if user u has interacted with item i (e.g., click). For convenience, we define the number of interactions of an item as $r_i = \sum_{u \in \mathcal{U}} y_{ui}$, and collect r_i over all items as a popularity vector \mathbf{r} . RS targets to suggest items to users based on their potential interests.

Recommendation Models. Embedding-based models are widely utilized in RS [58]. Such models convert user/item attributes (e.g., IDs) into d -dimensional representations ($\mathbf{u}_u, \mathbf{v}_i$), and make predictions using the embedding similarity [58]. Given that the inner product is a conventional similarity metric due to its efficiency in retrieval and superior performance [57, 61, 34], this work also focuses on the inner product for analysis. Specifically, the model’s predicted scores can be formulated as $\hat{y}_{ui} = \mu(\mathbf{u}_u^\top \mathbf{v}_i)$, where $\mu(\cdot)$ denotes an activation function like Sigmoid. \hat{y}_{ui} represents a user’s preference for an item, which is then used for ranking to generate recommendations. For clarity of presentation, we also employ matrix notation. Let matrices $\hat{\mathbf{Y}}, \mathbf{U}, \mathbf{V}$ represent scores over all user-item combinations, embeddings over all users and items, respectively. Model predictions can be succinctly expressed as $\hat{\mathbf{Y}} = \mu(\mathbf{UV}^\top)$.

Objective Functions. Common choices of loss functions for training a recommendation model include point-wise loss such as BCE and MSE [45], and pair-wise loss like BPR [46]. It is worth noting that BPR can be reconceptualized as a specialized pointwise loss if we construct hyper-item spaces and consider a pair of items as a unique hyper-item (please refer to Appendix A.1.1 for more details). As such, for convenience, this work focuses on point-wise loss for analysis. But we also discuss how our proposed debiased method adapts to BPR loss (Appendix A.1.2) and validate its effectiveness through experiments (Section 5).

Popularity Bias Amplification. Items’ interaction frequency in recommendation data often follows a long-tailed distribution [8, 17, 51]. For instance, in a typical Douban dataset, a mere 20% of the most popular items account for 86.3% of all interactions. When models are trained on such skewed data, they tend to absorb and amplify this bias, frequently over-prioritizing popular items in their recommendations. For example, in the Douban dataset using the MF model, 20% of the most popular items occupy over 99.7% of the recommendation slots, while a mere 0.6% of the most popular items occupy more than 63% (cf. Appendix B.1 more examples). This notorious effect significantly impacts the recommendation accuracy and fairness, even potentially posing detrimental effects on the entire ecosystem of RS[12]. Thus, understanding the underlying mechanisms behind this effect is crucial.

3 Understanding Popularity Bias Amplification

3.1 Popularity Bias Memorization Effect

3.1.1 Empirical Study. To discern how recommendation models memorize item popularity, we designed the following experiment: 1) We well trained three representative recommendation models, MF [38], LightGCN [27] and XSimGCL [62], on three real-world datasets (cf. Section 5 for experimental details); 2) We then performed SVD decomposition on the predicted score matrix, $\hat{\mathbf{Y}} = \mathbf{P}\Sigma\mathbf{Q}^\top = \sum_{1 \leq k \leq L} \sigma_k \mathbf{p}_k \mathbf{q}_k^\top$ where $L = \min(n, m)$ and $\sigma_1 \geq \sigma_2 \geq \dots \geq \sigma_L$. We further computed cosine similarity between the right principal singular vector \mathbf{q}_1 and the item popularity \mathbf{r} . The outcomes are showcased in Table 1. From these experiments, we draw an impressive observation:

Observation 1. *The principal right singular vector \mathbf{q}_1 of the matrix $\hat{\mathbf{Y}}$ aligns significantly with the item popularity \mathbf{r} . The cosine similarity consistently surpasses 0.98 over multiple recommendation models and datasets.*

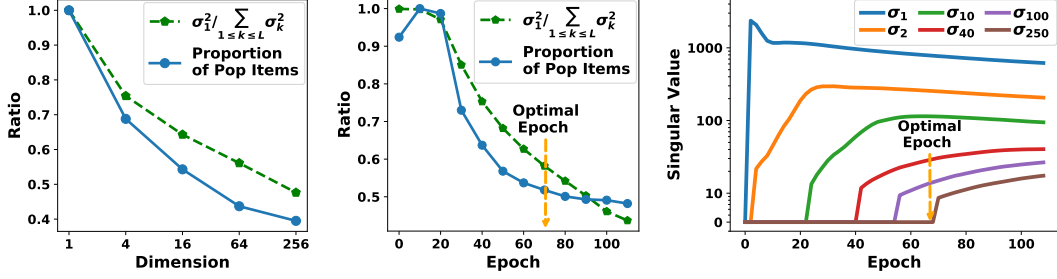
Given the orthogonal nature of different singular vectors, we can deduce that item popularity is almost entirely captured in the principal spectrum. This intriguing phenomenon elucidates how the recommendation model assimilates item popularity from the data and how this popularity influences recommendation outcomes.

3.1.2 Theoretical Analyses. Prior to the theoretical validation of observation 1, we posit a power-law hypothesis pertaining to recommendation data:

Hypothesis 1. *The interaction frequency of items in recommendation data follows a power-law distribution (a.k.a. Zipf law) described by $r_g \propto g^{-\alpha}$.*

Table 1: The cosine similarity between the principal singular vector (\mathbf{q}_1) and the item popularity (\mathbf{r}) under different backbones and loss functions.

Backbone	Movielens			Douban			Globo		
	MSE	BCE	BPR	MSE	BCE	BPR	MSE	BCE	BPR
MF	0.993	0.988	0.991	0.992	0.991	0.993	0.993	0.989	0.992
LightGCN	0.992	0.991	0.992	0.990	0.988	0.990	0.992	0.990	0.991
XSimGCL	0.998	0.994	0.995	0.991	0.990	0.992	0.992	0.985	0.989



(a) Exploring dimensions. (b) Exploring different epochs. (c) Exploring singular values.

Figure 2: Illustration of how dimension collapse impacts popularity bias in Movielens: (a)-(b) the proportion of popular items in recommendations and the ratio of the largest singular value ($\sigma_1^2 / \sum_{1 \leq k \leq L} \sigma_k^2$) with varying embedding dimensions and training epochs, respectively; (c) how singular values evolves during training.

Here r_g signifies the popularity of the g -th most popular item, and α is a shape parameter indicating the distribution’s slope. Power-law, as a typical long-tailed distribution, is prevalent across various natural and man-made phenomena [16]. Recent studies assert that item popularity in RS also aligns with this ubiquitous principle [8, 17, 51]. Then we have the following important theorem:

Theorem 1 (Popularity Memorization Effect). *Given an embedding-based recommendation model with sufficient capacity, when training the model on the data with power-law item popularity, the cosine similarity between item popularity \mathbf{r} and the principal singular vector \mathbf{q}_1 of the predicted score matrix is bounded with:*

$$\cos(\mathbf{r}, \mathbf{q}_1) \geq \frac{\sigma_1^2}{r_{\max} \sqrt{\zeta(2\alpha)}} \sqrt{1 - \frac{r_{\max}(\zeta(\alpha) - 1)}{\sigma_1^2}} \quad (1)$$

For $\alpha > 2$, this can be further bounded with:

$$\cos(\mathbf{r}, \mathbf{q}_1) \geq \sqrt{\frac{2 - \zeta(\alpha)}{\zeta(2\alpha)}} \quad (2)$$

where r_{\max} is the popularity of the most popular item, and $\zeta(\alpha)$ is Riemann zeta function with $\zeta(\alpha) = \sum_{j=1}^{\infty} \frac{1}{j^\alpha}$.

Proof can be found in Appendix A.2. Notably, as the long-tailed nature of item popularity intensifies (i.e., $\alpha \rightarrow \infty$ suggesting $\zeta(\alpha) \rightarrow 1$), the right side of Eq. (2) converges to one, implying a near-perfect alignment between \mathbf{r} and \mathbf{q}_1 . Even when the data isn’t markedly skewed and has a considerable $\zeta(\alpha)$, we typically observe σ_1^2 to vastly exceed r_{\max} , e.g., 5.6×10^5 vs. 4.6×10^3 in the dataset Movielens (with more examples presented in Appendix B.2). Thus, from Eq. (1), a high similarity between \mathbf{r} and \mathbf{q}_1 emerges. This theorem provides theoretical validation for our observation 1.

3.2 Popularity Bias Amplification Effect

Earlier discussions illuminate that the principal spectrum memorizes item popularity. In this subsection, we reveal the phenomenon of dimension collapse in recommendation systems (RS), which amplifies the effect of the principal spectrum, leading to popularity bias amplification.

3.2.1 Empirical Study. The occurrence of dimension collapse in RS is largely attributable to two factors: 1) explicit low-rank configuration of user/item embeddings [39, 27], and 2) intrinsic training dynamics associated with gradient-based optimization [15, 48, 6]. Here, we present experiments to validate these points and examine their impacts on popularity bias.

Impact of Low-Rank Configuration. Figure 2(a) displays the proportion of popular items in recommendations from well-trained MF models with varying embedding dimensions d . We also present the magnitude of the largest singular value σ_1 compared with other singular values. We report $\sigma_1^2 / \sum_{1 \leq k \leq L} \sigma_k^2$ as it is easily calculable, where the denominator equals the sum of the diagonal elements of $\hat{\mathbf{Y}}$. We observe:

Observation 2. *As the embedding dimension d decreases, the relative prominence of the principal singular value increases ($\sigma_1^2 / \sum_{1 \leq k \leq L} \sigma_k^2 \uparrow$) and the recommendation increasingly favors popular items.*

This observation reveals the impact of low-rank embeddings. A smaller d squeezes the dimensions (causing singular values of more dimensions to become zero), thereby relatively amplifying the effect of the principal spectrum. Consequently, item popularity contributes more significantly to ranking, resulting in more severe popularity bias.

Dimension Collapse from Gradient Optimization. Figure 2(c) illustrates the evolution of singular values as training progresses using a gradient-based optimizer; and Figure 2(b) offers a dynamic view of popularity bias and the ratio $\sigma_1^2 / \sum_{1 \leq k \leq L} \sigma_k^2$ over the training procedure. We observe:

Observation 3. *The principal singular value grows preferentially and swiftly, while others exhibit a more gradual increment. Notably, many singular values appear to be far from convergence even at the end of the training process. Accordingly, popularity bias is severe at the beginning but exhibits a relative decline as training advances. But even at the end of training, unless an extensive number of epochs are employed (which could result in computational overhead and potential over-fitting), the bias remains pronounced.*

This phenomenon reveals the dynamic of singular values during gradient optimization — the principal dimension is prioritized, while singular values of other dimensions are easily under-estimated. This inherent mechanism could readily lead to dimension collapse, relatively enhancing the impact of the principal spectrum, and thereby inducing popularity bias.

3.2.2 Theoretical Analyses. In this subsection, we focus on establishing a theoretical relationship between singular values and the ratio of popular items in recommendations. For readers interested in the theoretical support of the impact of gradient optimization, we refer them to the Appendix A.4, which are relatively straightforward by invoking recent gradient theory [15, 48]. For convenience, our analysis here concentrates on the ratio of the most popular item in top-1 recommendations. We have:

Theorem 2 (Popularity bias amplification). *Given hypothesis 1 and nearly perfect alignment between \mathbf{q}_1 and \mathbf{r} , the ratio of the most popular item in top-1 recommendations over all users is bounded by:*

$$\eta \geq \frac{1}{n} \phi \left(\frac{\sqrt{2\zeta(2\alpha)}}{1-2^{-\alpha}} \left(\frac{\sum_{1 \leq k \leq L} \sigma_k}{\sigma_1} - 1 \right) \right) \quad (3)$$

where $\phi(a) = \sum_{u \in \mathcal{U}} \mathbf{I}[p_{1u} > a]$ is an inverse cumulative function calculating the number of elements p_{1u} in the left principal singular vector \mathbf{p}_1 exceeding a given value a , and the function $\mathbf{I}[\cdot]$ signifies an indicator function.

The detailed proof is available in Appendix A.3. This theorem vividly showcases the influence of dimension collapse on popularity bias. Essentially, as dimension collapse intensifies the relative prominence of the principle singular value (i.e., $\frac{\sigma_1}{\sum_{1 \leq k \leq L} \sigma_k} \uparrow$), the input of the function $\phi(\cdot)$ decreases (i.e., $\frac{\sqrt{2\zeta(2\alpha)}}{1-2^{-\alpha}} \left(\frac{\sum_{1 \leq k \leq L} \sigma_k}{\sigma_1} - 1 \right) \downarrow$). Given the monotonically decreasing nature of $\phi(\cdot)$, dimension collapse thus escalates the ratio of most popular items in recommendations. Interestingly, the theorem illustrates the impact of a long-tailed distribution on popularity bias. A larger α (indicating a more skewed item popularity distribution) decreases the value of $\frac{\sqrt{2\zeta(2\alpha)}}{1-2^{-\alpha}}$, further elevating the lower bound of the ratio, intensifying bias.

4 Proposed Method

4.1 ReSN: Regulation with Spectral Norm

The above analyses elucidate the essence of the popularity bias amplification — the undue influence of the principal spectrum. To counteract this, we propose ReSN with leveraging *Spectral Norm* Regularizer to penalize the magnitude of principal singular value:

$$\mathcal{L}_{\text{ReSN}} = \mathcal{L}_R(\mathbf{Y}, \hat{\mathbf{Y}}) + \beta \|\hat{\mathbf{Y}}\|_2^2 \quad (4)$$

where $\mathcal{L}_R(\mathbf{Y}, \hat{\mathbf{Y}})$ is original recommendation loss, and $\|\cdot\|_2$ denote the spectral norm of a matrix measuring its principle singular value; β controls the contribution from the regularizer.

However, there are practical challenges: 1) the $n \times m$ dimensional matrix $\hat{\mathbf{Y}}$ can become exceptionally large, often comprising billions of entries, making direct calculations computationally untenable; 2)

Existing methods to determine the gradient of the spectral norm are iterative [60, 52], which further adds computational overhead.

To circumvent these challenges, we make two refinements: Firstly, given the alignment of the principal singular vector \mathbf{q}_1 with item popularity \mathbf{r} , the calculating of the spectral norm can be simplified into: $\|\hat{\mathbf{Y}}\|_2^2 = \|\hat{\mathbf{Y}}\mathbf{q}_1\|^2 \approx \|\hat{\mathbf{Y}}\mathbf{r}\|^2/\|\mathbf{r}\|^2$, where $\|\cdot\|$ denotes the L2-norm of a vector. It transforms the calculation of the complex spectral norm of a matrix to a simple L2-norm of a vector, avoiding iterative algorithms by leveraging the singular vector property. Further, the item popularity \mathbf{r} can be quickly computed via $\mathbf{r} = \mathbf{Y}^\top \mathbf{e}$, where \mathbf{e} represents a n -dimension vector filled with ones. Secondly, we exploit the low-rank nature of the matrix $\hat{\mathbf{Y}}$. For models based on embeddings, $\hat{\mathbf{Y}}$ can be expressed as $\hat{\mathbf{Y}} = \mu(\mathbf{UV}^\top)$, where \mathbf{U} and \mathbf{V} represent the embeddings associated with users and items, respectively, and $\mu(\cdot)$ designates an activation function. Our approach turns to penalize the spectral norm of the matrix before the introduction of the activation function. This is motivated by the ease of computation: $\|\mathbf{UV}^\top\|_2^2 = \|\mathbf{U}(\mathbf{V}^\top \tilde{\mathbf{q}}_1)\|^2$, where $\tilde{\mathbf{q}}_1$ denotes the right principal vector of the matrix \mathbf{UV}^\top . By adopting this method, we circumvent the computationally-intensive task of processing the entire matrix $\hat{\mathbf{Y}}$. Nonetheless, this method introduces a challenge: accurately computing $\tilde{\mathbf{q}}_1$, since it doesn't inherently align with item popularity. To rectify this, we may simply mirror the calculation of $\mathbf{q}_1 \leftarrow \frac{\mathbf{Y}^\top \mathbf{e}}{\|\mathbf{Y}^\top \mathbf{e}\|}$ to $\tilde{\mathbf{q}}_1 \leftarrow \frac{\mathbf{VU}^\top \mathbf{e}}{\|\mathbf{VU}^\top \mathbf{e}\|}$. This approach is clued by our Observation 1 and Theorem 1: a matrix's principal singular vector tends to align with the column sum vector, especially when the vector showcases a long-tailed distribution. The discussions presented in Appendix B.3 validate the precision of this strategy. In essence, our ReSN optimizes the following loss function:

$$\tilde{\mathcal{L}}_{\text{ReSN}} = \mathcal{L}_R(\mathbf{Y}, \hat{\mathbf{Y}}) + \frac{\beta}{\|\mathbf{VU}^\top \mathbf{e}\|^2} \|\mathbf{UV}^\top \mathbf{VU}^\top \mathbf{e}\|^2 \quad (5)$$

4.2 Discussions

The proposed ReSN have the following merits: 1) **Model-Agnostic**. The proposed ReSN is model-agnostic and easy to implement. Given that ReSN introduces merely a regularization term, it can be easily plugged into existing embedding-based methods with minimal code augmentation. 2) **Efficiency**. The regularizer can be fast computed from right to left — it predominantly requires the multiplication of a $n \times d$ (or $m \times d$) matrix with a vector. With a time complexity of $O((n + m)d)$, ReSN is highly efficient. Appendix B.5 also provides empirical evidence. The additional time for calculating the regularizer is negligible. 3) **Suitable for BPR Loss**. As delineated in Section 2, while BPR can be regarded as a specialized point-wise loss, it involves the concept of hyper-items. Our theoretical analyses presented in Appendix A.1.2 demonstrate ReSN can be a logical regularizer even for the BPR loss.

Compared with Other Regularizers: 1) recent studies [9, 69, 53] has employed regularizers to alleviate the dimensional collapse of user/item embeddings. Our ReSN diverges from these methods in two key aspects: Firstly, ReSN imposes constraints directly onto the prediction matrix, unlike the embedding matrix constraints utilized in these methods. This distinction is of significance due to the inherent spectral gap between the embeddings and the prediction matrix. Secondly, ReSN explicitly modulates the influence of the principal spectrum that captures popularity information, while these methods mainly focuses on promoting embedding uniformity. ReSN directly and solely mitigates the impact of the memorized popularity signal, thus demonstrating high efficacy in mitigating popularity bias; while others may disrupt the spectral structure of the prediction, potentially compromising model accuracy. 2) Other researchers have introduced various regularizers tailored to combat popularity bias [74, 36, 47]. However, these approaches are often heuristic, applying strong constraints to model predictions that may break the model's original spectrum. While it could mitigate popularity bias, this approach may also impair the model's ability to capture other useful signals, significantly compromising recommendation accuracy. Contrasting this, our ReSN is a light and theoretic-grounding approach — only modulates the influence of the principle spectrum.

Table 2: Performance comparison in terms of NDCG between ReSN and other baselines across seven datasets and three testing paradigms. The ‘‘Com’’(refers to ‘‘Common’’) represents the paradigm where the training and test datasets are partitioned randomly; ‘‘Deb’’(refers to ‘‘Debiased’’) represents the paradigm where a debiased test dataset is formulated based on item popularity; ‘‘Uni’’(refers to ‘‘Uniform-exposure’’) represents the paradigm where the test data is uniformly-exposed. The best result is bolded and the runner-up is underlined. The mark ‘*’ denotes the improvement achieved by ReSN over best baseline is significant with $p < 0.05$.

	Movielens		Douban		Yelp2018		Gowalla		Globo		Yahoo	Coat
	Com	Deb	Com	Deb	Com	Deb	Com	Deb	Com	Deb	Uni	Uni
MF	0.3572	0.1490	0.0440	0.0116	0.0416	0.0164	0.1182	0.0438	0.1709	0.0028	0.6672	0.5551
Zerosum	0.3309	0.1411	0.0434	0.0110	0.0415	0.0137	0.1063	0.0421	0.1630	0.0036	0.6665	0.5633
MACR	<u>0.3732</u>	0.1647	0.0441	0.0145	0.0404	0.0208	0.1107	0.0545	0.1782	<u>0.0253</u>	0.6714	0.5661
PDA	0.3688	<u>0.1662</u>	0.0446	0.0171	<u>0.0437</u>	<u>0.0229</u>	0.1283	<u>0.0675</u>	<u>0.1725</u>	0.0243	<u>0.6756</u>	0.5676
InvCF	0.3723	0.1567	<u>0.0450</u>	0.0152	0.0433	0.0183	0.1302	0.0592	0.1671	0.0194	0.6519	<u>0.5715</u>
IPL	0.3618	0.1621	0.0442	<u>0.0173</u>	0.0419	0.0219	<u>0.1318</u>	0.0623	0.1715	0.0203	0.6691	<u>0.5602</u>
ReSN	0.3857*	0.1745*	0.0456*	0.0186*	0.0445*	0.0254*	0.1343*	0.0703*	0.1682	0.0256*	0.6792*	0.5871*

5 Experiments

5.1 Experiment Settings

Datasets and Metrics. We adopt seven real-world datasets, Yelp2018 [27], Douban [50], Movielens [63], Gowalla [26], Globo [20], Yahoo!R3 [38] and Coat [49] for evaluating our model performance. Details about these datasets refer to C.1.

We adopt three representative testing paradigms for comprehensive evaluations: 1) **Common:** We employ the conventional testing paradigm in RS, wherein the datasets are randomly partitioned into training (70%), validation (10%), and testing (20%). We also report the accuracy-fairness trade-off in this setting. 2) **Debiased:** Closely referring to [56, 7, 71], we sample a debiased test set where items are uniformly distributed, aiming to evaluate the model’s efficacy in mitigating popularity bias. 3) **Uniform-exposure:** We also adopt the uniform exposure paradigm for model testing as the recent work [64]. Notably, the datasets Yahoo!R3 and Coat contain a small dataset collected through a random recommendation policy. Such data isolate the popularity bias from uneven exposure, offering a more precise estimation of user preferences. Consequently, we train our recommendation model on conventionally biased data and then test it on these uniformly-exposed data.

For evaluation metrics, we adopt the widely-used **NDCG@K** for evaluating accuracy [32]. We simply adopt $K = 5$ for Yahoo and Coat datasets and $K = 20$ for the other datasets as recent work [27, 64, 62]. We observe similar results with other metrics. We also employ the **ratio of pop/unpopular items** for illustrating the severity of popularity bias in recommendations. Here we closely refer to recent work [68] to define popular and unpopular items. We sort the items according to their popularity in descending order, and divide items into five groups ensuring the aggregated popularity of items within each group is the same. We define the items in the most popular groups as popular items, while the others as unpopular.

Baselines. The following methods are compared: 1) **MACR** (KDD’21 [56]), **PDA** (SIGIR’21 [68]): the representative causality-based debiasing methods, which posit a causal graph [42] for the recommendation procedure and leverage causal inference to mitigate popularity bias accordingly; 2) **InvCF** (WWW’23 [64]): the SOTA method that addresses popularity bias by disentangling the popularity from user preference. 3) **Zerosum** (Recsys’22 [47]), **IPL** (SIGIR’23 [36]): the representative methods based on regularizers, which penalize the score differences or constrain the ratio of the predicted preference with the exposure.

For fair comparisons, we implement all compared methods with uniform MF backbone and MSE loss. We also explore the performance with other backbones and losses in subsection 5.3. Besides above baselines, we also compare our method with the methods on mitigating dimension collapse, including nCL [9] and DirectAU [53]; and the debiasing methods tailored for GNN-based methods including APDA [73] and $GCF_{\log\det}$ [69] when using GNN-based backbones.

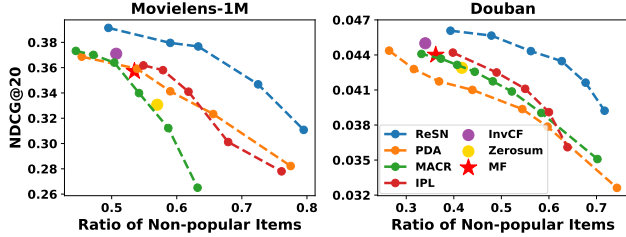


Figure 3: Pareto curves of compared methods illustrating the trade-off between accuracy and fairness.

Figure 4: NDCG@20 comparison with methods for addressing Dimension Collapse.

	Movielens	Douban	Gowalla
MF	0.1529	0.0116	0.0438
nCL	0.1572	0.0112	0.0451
DirectAU	<u>0.0169</u>	<u>0.0131</u>	<u>0.0622</u>
ReSN	0.1788	0.0188	0.0712

Parameter Settings. The embedding dimension d is 256 while other dimensions are explored in B.4. Grid search is utilized find the optimal hyperparameters. More details refer to Appendix C.2.

5.2 Performance Comparison (RQ1)

Comparison under three testing paradigms. Table 2 showcases the NDCG@K comparison across seven datasets over three testing paradigms. Under the Common testing paradigm, our ReSN, with few exceptions, consistently outperforms compared methods. This superior performance can be attributed to the rigorous theoretical foundations of ReSN, which pinpoint and address the root cause of bias amplification. By curbing this bias amplification, ReSN achieves significant improvements in recommendation accuracy. Transitioning to the Debaised and Uniform-exposure testing paradigms, the improvements by ReSN become even more impressive, demonstrating its effectiveness in mitigating popularity bias.

Exploring Accuracy-fairness Trade-off. Given the conventional accuracy-fairness trade-off observed in RS, we delve deeper into examining this effect across various methods. After well-training various methods with differing hyper-parameters (details of hyper-parameters tuning refer to Appendix C.2), we depict the Pareto frontier in Figure 3. It highlights the relationship between accuracy (NDCG@20) and fairness (ratio of unpopular items) under the Common testing paradigm. Here, positions in the top-right corner indicate superior performance. We observe that ReSN exhibits a more favorable Pareto curve in comparison to other baselines. When fairness is held constant, ReSN showcases superior accuracy. Conversely, when accuracy is fixed, ReSN delivers enhanced fairness. This suggests that ReSN effectively navigates the fairness-accuracy trade-off, primarily through its capability to counteract popularity bias amplification — it only mitigates the effect of the principle spectrum without disturbing other spectrum.

Compared with the Methods on Tackling Dimension Collapse. Table 4 shows the results of our ReSN compared with existing methods on tackling dimension collapse on debaised testing paradigm. nCL and DirectAU can indeed mitigate the popularity bias. However, their performance is inferior to ReSN. The reason is that our ReSN is designed for debiasing, directly modulating the effect of the item popularity on predictions, and thus yielding better performance.

5.3 Adaptability Exploration (RQ2)

To investigate the adaptability of ReSN, we evaluate it with various backbones and loss functions under debaised testing paradigm. Table 3 showcases the performance of ReSN under LightGCN [27] and XSimGCL [62], where APDA [73] and $GCF_{\log\det}$ [69] that tailored for GNN-based backbones are included. Besides, Table 5 depicts the results with BCE and BPR losses. Notably, ReSN consistently outperforms compared methods, irrespective of the chosen backbone or loss function. These findings affirm the great adaptability of ReSN, underscoring its ability to seamlessly integrate with diverse recommendation models. Our ReSN also outperforms those debiasing methods tailored for GNN-based methods. They reason is that they only consider to mitigate bias amplification raised by GNNs while ignoring the bias from the generic recommendation mechanism.

Table 3: NDCG@20 comparison with LightGCN and XSimGCL backbone.

	Movielens		Douban		Gowalla	
	LGCN	XSGCL	LGCN	XSGCL	LGCN	XSGCL
Backbone	0.1531	0.1686	0.0117	0.0132	0.0446	0.0563
Zerosum	0.1363	0.1438	0.0112	0.0129	0.0437	0.0498
MACR	0.1682	0.1692	0.0157	0.0164	0.0543	0.0623
PDA	<u>0.1684</u>	<u>0.1732</u>	<u>0.0182</u>	0.0190	<u>0.0689</u>	<u>0.0732</u>
InvCF	0.1602	0.1672	0.0153	0.0169	0.0599	0.0687
IPL	0.1653	0.1701	0.0166	<u>0.0193</u>	0.0642	0.0699
APDA	0.1657	0.1713	0.0156	0.0189	0.0468	0.0522
$GCF_{\log\det}$	0.1672	0.1724	0.0124	0.0141	0.0403	0.0492
ReSN	0.1758	0.1810	0.0194	0.0202	0.0717	0.0763

Figure 5: NDCG@20 comparison with different Loss functions.

	Movielens		Douban		Gowalla	
	+BCE	+BPR	+BCE	+BPR	+BCE	+BPR
MF	0.1529	0.1540	0.0117	0.0120	0.0432	0.0431
Zerosum	0.1472	0.1498	0.0109	0.0106	0.0423	0.0425
MACR	<u>0.1682</u>	0.1629	0.0155	0.0149	0.0574	0.0546
PDA	0.1635	<u>0.1633</u>	<u>0.0176</u>	0.0173	<u>0.0661</u>	<u>0.0675</u>
InvCF	0.1574	0.1582	0.0153	0.0154	0.0553	0.0583
IPL	0.1612	0.1628	0.0173	<u>0.0177</u>	0.0612	0.0626
ReSN	0.1788	0.1693	0.0188	0.0180	0.0712	0.0702

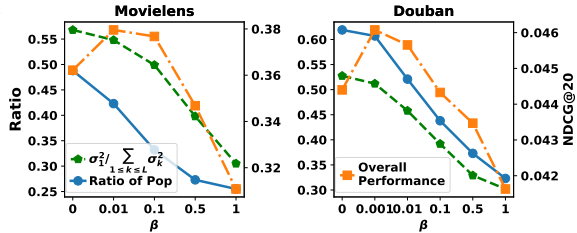


Figure 6: The proportion of popular items in recommendations and the ratio of the largest singular value ($\sigma_1^2 / \sum_{1 \leq k \leq L} \sigma_k^2$) and NDCG@20 with varying β .

5.4 Hyperparameter Study (RQ3)

Figure 6 presents the recommendation accuracy, the ratio of popular items, and the ratio of principle singular value ($\sigma_1^2 / \sum_{1 \leq k \leq L} \sigma_k^2$) in ReSN as the hyperparameter β varies. Notably, as β increases, the ratio of principle singular value and the severity of popularity bias reduces. This trend affirms the efficacy of our regularizer. Regarding recommendation accuracy, it initially rises and then declines with an increase in β . This can be attributed to the fact that popularity bias isn't intrinsically detrimental [68, 70]. Indeed, item popularity can also convey beneficial information about the item's appeal or quality, which ought to be retained. Hence, the strategic approach for popularity bias lies in mitigating its bias amplification, rather than eliminating it entirely. That is also our target.

6 Related Work

Analyses on Popularity Bias. In RS, items frequently exhibit a long-tailed distribution in terms of interaction frequency. Models trained on skewed data are susceptible to inheriting and exacerbating such bias [28, 74, 4, 5, 75]. The crux of tackling popularity bias lies in understanding why and how recommendation models intensify popularity bias. Several recent efforts aim to elucidate this. Among these, causality-based investigations stand out. For instance, Zhang et al. [68] developed a causal graph of the data generative process, attributing the amplification of popularity bias to a confounding effect; Wei et al. [56] presented an alternate causal graph, exploring the direct and indirect causal influence of popularity bias on predictions; Wang et al. [55] used yet another causal graph to highlight bias amplification, focusing on the impact of users' historical long-tailed distribution across item groups. Despite their contributions, a common limitation among these causality-based methods is their surface-level engagement with the causal relationships among variables, rather than delving deeper into the underlying mechanisms. For example, these studies usually operate on the assumption that item popularity directly affects predictions. However, the specifics of how and why predictions memorize and are influenced by item popularity remain largely unexplored. Worse still, their effectiveness hinges on the accuracy of their respective causal graphs, which might not always align with real-world scenarios due to the widespread presence of unmeasured confounders [21, 33].

There have been other theoretical investigations into popularity bias. For instance, Zhu et al. [74] demonstrate that model predictions inherit item popularity, yet they failed to elucidate the amplification. Also, their conclusions rely on a strong assumption that the preference scores maintain same distribution over different user-item pairs. The study by [41] shed light on the limited expressiveness of low-rank embeddings, giving clues of popularity bias in recommendations. Yet, they did not factor in the impact of long-tailed training data. In fact, popularity bias originates from long-tailed data [68, 74], amplified during training, which would be more serious than the theoretical analyses presented in [41]. Some efforts Chen et al. [13], Kim et al. [30] examined popularity bias through embedding magnitude, their theoretical analysis can only be applied in the early stages of training. Other researchers delved into how graph neural networks amplify popularity bias, whether through influence functions [10], the hub effect [73] or dimensional collapse [69]. However, their conclusions can not be extended to general recommendation models.

Methods on Tackling Popularity Bias. Recent efforts on addressing popularity bias are mainly four types: 1) Causality-driven methods assume a causal graph to identify popularity bias and employ causal inference techniques for rectification. While they have demonstrated efficacy, their success is closely tied to the accuracy of the causal graph. This poses challenges due to the prevalence of unmeasured confounders [21, 33, 40]. 2) Propensity-based methods [49, 25, 19, 66, 54] adjust the

data distribution by reweighting the training data instances. While this approach directly negates popularity bias in the data, it may inadvertently obscure other valuable signals, such as item quality. Consequently, these methods often underperform compared to causality-driven ones. 3) Regularizer-based methods [3, 74, 47, 36, 29] constrain predictions by introducing regularization terms. For example, Zhu et al. [74] employs a Pearson coefficient regularizer to diminish the correlation between item popularity and model predictions; Rhee et al. [47] proposes to regularize the score differences; [36] constrains the predictions with IPL criterion. As discussed in section 4.2, their constraints are too strong, may significantly compromising accuracy. 4) Disentanglement-based methods [64, 59, 14] target at learning disentangled embeddings that segregate the influence of popularity from genuine user preferences. While promising, achieving a perfect disentanglement of popularity bias from true preferences remains a formidable challenge in RS.

7 Conclusion and Limitation

In this study, we delve into the root cause of popularity bias amplification. Our analyses offer two core insights: 1) Item popularity is encoded in the principal spectrum of model predictions; 2) The phenomenon of dimension collapse accentuates the influence of the principal spectrum. Based on these insights, we introduce ReSN, an efficient technique aimed at mitigating popularity bias by penalizing the principle singular value. A potential limitation of our study pertains to the static perspective on popularity bias, neglecting its dynamic nature as it evolves temporally. It could be more insightful to investigate the mechanism of bias amplification in the context of temporal sequential recommendations, and to examine its evolution during the feedback loop.

References

- [1] Martín Abadi, Paul Barham, Jianmin Chen, Zhifeng Chen, Andy Davis, Jeffrey Dean, Matthieu Devin, Sanjay Ghemawat, Geoffrey Irving, Michael Isard, et al. {TensorFlow}: a system for {Large-Scale} machine learning. In *12th USENIX symposium on operating systems design and implementation (OSDI 16)*, pages 265–283, 2016.
- [2] Hervé Abdi and Lynne J Williams. Principal component analysis. *Wiley interdisciplinary reviews: computational statistics*, 2(4):433–459, 2010.
- [3] Himan Abdollahpouri, Robin Burke, and Bamshad Mobasher. Controlling popularity bias in learning-to-rank recommendation. In *Proceedings of the eleventh ACM conference on recommender systems*, pages 42–46, 2017.
- [4] Himan Abdollahpouri, Masoud Mansoury, Robin Burke, and Bamshad Mobasher. The impact of popularity bias on fairness and calibration in recommendation. *arXiv preprint arXiv:1910.05755*, 2019.
- [5] Himan Abdollahpouri, Masoud Mansoury, Robin Burke, and Bamshad Mobasher. The connection between popularity bias, calibration, and fairness in recommendation. In *Proceedings of the 14th ACM Conference on Recommender Systems*, pages 726–731, 2020.
- [6] Sanjeev Arora, Nadav Cohen, Wei Hu, and Yuping Luo. Implicit regularization in deep matrix factorization. *Advances in Neural Information Processing Systems*, 32, 2019.
- [7] Stephen Bonner and Flavian Vasile. Causal embeddings for recommendation. In *Proceedings of the 12th ACM conference on recommender systems*, pages 104–112, 2018.
- [8] Rodrigo Borges and Kostas Stefanidis. On measuring popularity bias in collaborative filtering data. In *Proceedings of the Workshops of the EDBT/ICDT 2020 Joint Conference, Copenhagen, Denmark, March 30, 2020*, volume 2578, 2020.
- [9] Huiyuan Chen, Vivian Lai, Hongye Jin, Zhimeng Jiang, Mahashweta Das, and Xia Hu. Towards mitigating dimensional collapse of representations in collaborative filtering. *arXiv preprint arXiv:2312.17468*, 2023.
- [10] Jiajia Chen, Jiancan Wu, Jiawei Chen, Xin Xin, Yong Li, and Xiangnan He. How graph convolutions amplify popularity bias for recommendation? *arXiv preprint arXiv:2305.14886*, 2023.
- [11] Jiajia Chen, Jiancan Wu, Jiawei Chen, Xin Xin, Yong Li, and Xiangnan He. How graph convolutions amplify popularity bias for recommendation? *Frontiers of Computer Science*, 18(5):185603, 2024.

- [12] Jiawei Chen, Hande Dong, Xiang Wang, Fuli Feng, Meng Wang, and Xiangnan He. Bias and debias in recommender system: A survey and future directions. *ACM Transactions on Information Systems*, 41(3): 1–39, 2023.
- [13] Jiawei Chen, Junkang Wu, Jiancan Wu, Xuezi Cao, Sheng Zhou, and Xiangnan He. Adap- τ : Adaptively modulating embedding magnitude for recommendation. In *Proceedings of the ACM Web Conference 2023*, pages 1085–1096, 2023.
- [14] Zhihong Chen, Jiawei Wu, Chenliang Li, Jingxu Chen, Rong Xiao, and Binqiang Zhao. Co-training disentangled domain adaptation network for leveraging popularity bias in recommenders. In *Proceedings of the 45th International ACM SIGIR Conference on Research and Development in Information Retrieval*, pages 60–69, 2022.
- [15] Hung-Hsu Chou, Carsten Gieshoff, Johannes Maly, and Holger Rauhut. Gradient descent for deep matrix factorization: Dynamics and implicit bias towards low rank. *Applied and Computational Harmonic Analysis*, page 101595, 2023.
- [16] Aaron Clauset, Cosma Rohilla Shalizi, and Mark EJ Newman. Power-law distributions in empirical data. *SIAM review*, 51(4):661–703, 2009.
- [17] Ludovik Çoba, Panagiotis Symeonidis, and Markus Zanker. Visual analysis of recommendation performance. In *Proceedings of the Eleventh ACM Conference on Recommender Systems*, pages 362–363, 2017.
- [18] Paul Covington, Jay Adams, and Emre Sargin. Deep neural networks for youtube recommendations. In *Proceedings of the 10th ACM conference on recommender systems*, pages 191–198, 2016.
- [19] Quanyu Dai, Zhenhua Dong, and Xu Chen. Debaised recommendation with neural stratification. *AI Open*, 3:213–217, 2022.
- [20] Gabriel de Souza Pereira Moreira, Felipe Ferreira, and Adilson Marques da Cunha. News session-based recommendations using deep neural networks. In *Proceedings of the 3rd workshop on deep learning for recommender systems*, pages 15–23, 2018.
- [21] Sihao Ding, Peng Wu, Fuli Feng, Yitong Wang, Xiangnan He, Yong Liao, and Yongdong Zhang. Addressing unmeasured confounder for recommendation with sensitivity analysis. In *Proceedings of the 28th ACM SIGKDD Conference on Knowledge Discovery and Data Mining*, pages 305–315, 2022.
- [22] Chongming Gao, Kexin Huang, Jiawei Chen, Yuan Zhang, Biao Li, Peng Jiang, Shiqi Wang, Zhong Zhang, and Xiangnan He. Alleviating matthew effect of offline reinforcement learning in interactive recommendation. In *Proceedings of the 46th International ACM SIGIR Conference on Research and Development in Information Retrieval*, page 238–248, 2023.
- [23] Chongming Gao, Shiqi Wang, Shijun Li, Jiawei Chen, Xiangnan He, Wenqiang Lei, Biao Li, Yuan Zhang, and Peng Jiang. Cirs: Bursting filter bubbles by counterfactual interactive recommender system. *ACM Transactions on Information Systems*, 42(1):1–27, 2023.
- [24] Xavier Glorot and Yoshua Bengio. Understanding the difficulty of training deep feedforward neural networks. In *Proceedings of the thirteenth international conference on artificial intelligence and statistics*, pages 249–256. JMLR Workshop and Conference Proceedings, 2010.
- [25] Alois Gruson, Praveen Chandar, Christophe Charbuillet, James McInerney, Samantha Hansen, Damien Tardieu, and Ben Carterette. Offline evaluation to make decisions about playlist recommendation algorithms. In *Proceedings of the Twelfth ACM International Conference on Web Search and Data Mining*, pages 420–428, 2019.
- [26] Xiangnan He, Lizi Liao, Hanwang Zhang, Liqiang Nie, Xia Hu, and Tat-Seng Chua. Neural collaborative filtering. In *Proceedings of the 26th international conference on world wide web*, pages 173–182, 2017.
- [27] Xiangnan He, Kuan Deng, Xiang Wang, Yan Li, Yongdong Zhang, and Meng Wang. Lightgcn: Simplifying and powering graph convolution network for recommendation. In *Proceedings of the 43rd International ACM SIGIR conference on research and development in Information Retrieval*, pages 639–648, 2020.
- [28] Dietmar Jannach, Lukas Lerche, Iman Kamehkhosh, and Michael Jugovac. What recommenders recommend: an analysis of recommendation biases and possible countermeasures. *User Modeling and User-Adapted Interaction*, 25:427–491, 2015.

- [29] Jiarui Jin, Zexue He, Mengyue Yang, Weinan Zhang, Yong Yu, Jun Wang, and Julian McAuley. Inforank: Unbiased learning-to-rank via conditional mutual information minimization. In *Proceedings of the ACM on Web Conference 2024*, page 1350–1361, 2024.
- [30] Dain Kim, Jinhyeok Park, and Dongwoo Kim. Test time embedding normalization for popularity bias mitigation. *arXiv preprint arXiv:2308.11288*, 2023.
- [31] DP Kingma. Adam: a method for stochastic optimization. In *Int Conf Learn Represent*, 2014.
- [32] Walid Krichene and Steffen Rendle. On sampled metrics for item recommendation. In *Proceedings of the 26th ACM SIGKDD international conference on knowledge discovery & data mining*, pages 1748–1757, 2020.
- [33] Haoxuan Li, Yanghao Xiao, Chunyuan Zheng, and Peng Wu. Balancing unobserved confounding with a few unbiased ratings in debiased recommendations. In *Proceedings of the ACM Web Conference 2023*, pages 1305–1313, 2023.
- [34] Zihan Lin, Changxin Tian, Yupeng Hou, and Wayne Xin Zhao. Improving graph collaborative filtering with neighborhood-enriched contrastive learning. In *Proceedings of the ACM Web Conference 2022*, pages 2320–2329, 2022.
- [35] Seppo Linnainmaa. Taylor expansion of the accumulated rounding error. *BIT Numerical Mathematics*, 16(2):146–160, 1976.
- [36] Yuanhao Liu, Qi Cao, Huawei Shen, Yunfan Wu, Shuchang Tao, and Xueqi Cheng. Popularity debiasing from exposure to interaction in collaborative filtering. In *Proceedings of the 46th International ACM SIGIR Conference on Research and Development in Information Retrieval*, page 1801–1805, 2023.
- [37] Masoud Mansoury, Himan Abdollahpouri, Mykola Pechenizkiy, Bamshad Mobasher, and Robin Burke. Feedback loop and bias amplification in recommender systems. In *Proceedings of the 29th ACM international conference on information & knowledge management*, pages 2145–2148, 2020.
- [38] Benjamin M Marlin and Richard S Zemel. Collaborative prediction and ranking with non-random missing data. In *Proceedings of the third ACM conference on Recommender systems*, pages 5–12, 2009.
- [39] Andriy Mnih and Russ R Salakhutdinov. Probabilistic matrix factorization. *Advances in neural information processing systems*, 20, 2007.
- [40] Wentao Ning, Reynold Cheng, Xiao Yan, Ben Kao, Nan Huo, Nur Al Hasan Haldar, and Bo Tang. Debiasing recommendation with personal popularity. In *Proceedings of the ACM on Web Conference 2024*, page 3400–3409, 2024.
- [41] Naoto Ohsaka and Riku Togashi. Curse of "low" dimensionality in recommender systems. In *Proceedings of the 46th International ACM SIGIR Conference on Research and Development in Information Retrieval*, page 537–547, 2023.
- [42] Judea Pearl. *Causality*. Cambridge university press, 2009.
- [43] S Unnikrishna Pillai, Torsten Suel, and Seunghun Cha. The perron-frobenius theorem: some of its applications. *IEEE Signal Processing Magazine*, 22(2):62–75, 2005.
- [44] Jiezhong Qiu, Jian Tang, Hao Ma, Yuxiao Dong, Kuansan Wang, and Jie Tang. Deepinf: Social influence prediction with deep learning. In *Proceedings of the 24th ACM SIGKDD International Conference on Knowledge Discovery & Data Mining*, pages 2110–2119, 2018.
- [45] Steffen Rendle. Item recommendation from implicit feedback. In *Recommender Systems Handbook*. Springer, 2022.
- [46] Steffen Rendle, Christoph Freudenthaler, Zeno Gantner, and Lars Schmidt-Thieme. Bpr: Bayesian personalized ranking from implicit feedback. In *Proceedings of the Twenty-Fifth Conference on Uncertainty in Artificial Intelligence*, pages 452–461, 2009.
- [47] Wondo Rhee, Sung Min Cho, and Bongwon Suh. Countering popularity bias by regularizing score differences. In *Proceedings of the 16th ACM Conference on Recommender Systems*, pages 145–155, 2022.
- [48] Andrew M Saxe, James L McClelland, and Surya Ganguli. A mathematical theory of semantic development in deep neural networks. *Proceedings of the National Academy of Sciences*, 116(23):11537–11546, 2019.

- [49] Tobias Schnabel, Adith Swaminathan, Ashudeep Singh, Navin Chandak, and Thorsten Joachims. Recommendations as treatments: Debiasing learning and evaluation. In *international conference on machine learning*, pages 1670–1679. PMLR, 2016.
- [50] Weiping Song, Zhiping Xiao, Yifan Wang, Laurent Charlin, Ming Zhang, and Jian Tang. Session-based social recommendation via dynamic graph attention networks. In *Proceedings of the Twelfth ACM international conference on web search and data mining*, pages 555–563, 2019.
- [51] Harald Steck. Item popularity and recommendation accuracy. In *Proceedings of the fifth ACM conference on Recommender systems*, pages 125–132, 2011.
- [52] Shuhan Sun, Zhiyong Xu, and Jianlin Zhang. Spectral norm regularization for blind image deblurring. *Symmetry*, 13(10):1856, 2021.
- [53] Chenyang Wang, Yuanqing Yu, Weizhi Ma, Min Zhang, Chong Chen, Yiqun Liu, and Shaoping Ma. Towards representation alignment and uniformity in collaborative filtering. In *Proceedings of the 28th ACM SIGKDD Conference on Knowledge Discovery and Data Mining*, pages 1816–1825, 2022.
- [54] Lei Wang, Chen Ma, Xian Wu, Zhaopeng Qiu, Yefeng Zheng, and Xu Chen. Causally debiased time-aware recommendation. In *Proceedings of the ACM on Web Conference 2024*, page 3331–3342, 2024.
- [55] Wenjie Wang, Fuli Feng, Xiangnan He, Xiang Wang, and Tat-Seng Chua. Deconfounded recommendation for alleviating bias amplification. In *Proceedings of the 27th ACM SIGKDD Conference on Knowledge Discovery & Data Mining*, pages 1717–1725, 2021.
- [56] Tianxin Wei, Fuli Feng, Jiawei Chen, Ziwei Wu, Jinfeng Yi, and Xiangnan He. Model-agnostic counterfactual reasoning for eliminating popularity bias in recommender system. In *Proceedings of the 27th ACM SIGKDD Conference on Knowledge Discovery & Data Mining*, pages 1791–1800, 2021.
- [57] Jiancan Wu, Xiang Wang, Fuli Feng, Xiangnan He, Liang Chen, Jianxun Lian, and Xing Xie. Self-supervised graph learning for recommendation. In *Proceedings of the 44th international ACM SIGIR conference on research and development in information retrieval*, pages 726–735, 2021.
- [58] Le Wu, Xiangnan He, Xiang Wang, Kun Zhang, and Meng Wang. A survey on accuracy-oriented neural recommendation: From collaborative filtering to information-rich recommendation. *IEEE Transactions on Knowledge and Data Engineering*, 35(5):4425–4445, 2022.
- [59] Guipeng Xv, Chen Lin, Hui Li, Jinsong Su, Weiyao Ye, and Yewang Chen. Neutralizing popularity bias in recommendation models. In *Proceedings of the 45th International ACM SIGIR Conference on Research and Development in Information Retrieval*, pages 2623–2628, 2022.
- [60] Yuichi Yoshida and Takeru Miyato. Spectral norm regularization for improving the generalizability of deep learning. *arXiv preprint arXiv:1705.10941*, 2017.
- [61] Junliang Yu, Hongzhi Yin, Xin Xia, Tong Chen, Lizhen Cui, and Quoc Viet Hung Nguyen. Are graph augmentations necessary? simple graph contrastive learning for recommendation. In *Proceedings of the 45th international ACM SIGIR conference on research and development in information retrieval*, pages 1294–1303, 2022.
- [62] Junliang Yu, Xin Xia, Tong Chen, Lizhen Cui, Nguyen Quoc Viet Hung, and Hongzhi Yin. Xsimgcl: Towards extremely simple graph contrastive learning for recommendation. *IEEE Transactions on Knowledge and Data Engineering*, 2023.
- [63] Wenhui Yu and Zheng Qin. Graph convolutional network for recommendation with low-pass collaborative filters. In *International Conference on Machine Learning*, pages 10936–10945. PMLR, 2020.
- [64] An Zhang, Jingnan Zheng, Xiang Wang, Yancheng Yuan, and Tat-Seng Chua. Invariant collaborative filtering to popularity distribution shift. In *Proceedings of the ACM Web Conference 2023*, pages 1240–1251, 2023.
- [65] An Zhang, Wenchang Ma, Pengbo Wei, Leheng Sheng, and Xiang Wang. General debiasing for graph-based collaborative filtering via adversarial graph dropout. In *Proceedings of the ACM on Web Conference 2024*, page 3864–3875, 2024.
- [66] Fan Zhang and Qijie Shen. A model-agnostic popularity debias training framework for click-through rate prediction in recommender system. In *Proceedings of the 46th International ACM SIGIR Conference on Research and Development in Information Retrieval*, pages 1760–1764, 2023.

- [67] Xiang Zhang, Douglas E Faries, Hu Li, James D Stamey, and Guido W Imbens. Addressing unmeasured confounding in comparative observational research. *Pharmacoepidemiology and drug safety*, 27(4): 373–382, 2018.
- [68] Yang Zhang, Fuli Feng, Xiangnan He, Tianxin Wei, Chonggang Song, Guohui Ling, and Yongdong Zhang. Causal intervention for leveraging popularity bias in recommendation. In *Proceedings of the 44th International ACM SIGIR Conference on Research and Development in Information Retrieval*, pages 11–20, 2021.
- [69] Yifei Zhang, Hao Zhu, Zixing Song, Piotr Koniusz, Irwin King, et al. Mitigating the popularity bias of graph collaborative filtering: A dimensional collapse perspective. In *Thirty-seventh Conference on Neural Information Processing Systems*, 2023.
- [70] Zihao Zhao, Jiawei Chen, Sheng Zhou, Xiangnan He, Xuezhi Cao, Fuzheng Zhang, and Wei Wu. Popularity bias is not always evil: Disentangling benign and harmful bias for recommendation. *IEEE Transactions on Knowledge and Data Engineering*, 2022.
- [71] Yu Zheng, Chen Gao, Xiang Li, Xiangnan He, Yong Li, and Depeng Jin. Disentangling user interest and conformity for recommendation with causal embedding. In *Proceedings of the Web Conference 2021*, pages 2980–2991, 2021.
- [72] Guorui Zhou, Xiaoqiang Zhu, Chenru Song, Ying Fan, Han Zhu, Xiao Ma, Yanghui Yan, Junqi Jin, Han Li, and Kun Gai. Deep interest network for click-through rate prediction. In *Proceedings of the 24th ACM SIGKDD international conference on knowledge discovery & data mining*, pages 1059–1068, 2018.
- [73] Huachi Zhou, Hao Chen, Junnan Dong, Daochen Zha, Chuang Zhou, and Xiao Huang. Adaptive popularity debiasing aggregator for graph collaborative filtering. pages 7–17, 2023.
- [74] Ziwei Zhu, Yun He, Xing Zhao, Yin Zhang, Jianling Wang, and James Caverlee. Popularity-opportunity bias in collaborative filtering. In *Proceedings of the 14th ACM International Conference on Web Search and Data Mining*, pages 85–93, 2021.
- [75] Ziwei Zhu, Yun He, Xing Zhao, and James Caverlee. Evolution of popularity bias: Empirical study and debiasing. *arXiv preprint arXiv:2207.03372*, 2022.

A Theoretical Analysis

A.1 Analysis of BPR loss

A.1.1 Reconceptualizing from the BPR to the BCE loss

BPR loss is expressed as:

$$\mathcal{L}_{BPR} = - \sum_{u \in \mathcal{U}} \sum_{i \in \mathcal{I}, y_{ui}=1} \sum_{j \in \mathcal{I}, y_{uj}=0} \log(\mu(\mathbf{u}_u^\top \mathbf{v}_i - \mathbf{u}_u^\top \mathbf{v}_j)) \quad (6)$$

Then we can construct a hyper-item space denoted as $\mathcal{I}' = \mathcal{I} \times \mathcal{I}$ derived from item pairs, and define the embeddings of hyper-items as $\mathbf{v}'_{ij} = \mathbf{v}_i - \mathbf{v}_j$ and assign new observed interactions to the combinations of users and hyper-items, *i.e.*, $y'_{u,ij} = 1$ for $y_{ui} = 1 \& y_{uj} = 0$ and $y'_{u,ij} = 0$ for $y_{ui} = 0 \& y_{uj} = 1$.

With this transformation, the BPR loss can be effectively reframed as:

$$\begin{aligned} \mathcal{L}_{BPR} &= - \sum_{u \in \mathcal{U}} \sum_{i \in \mathcal{I}, y_{ui}=1} \sum_{j \in \mathcal{I}, y_{uj}=0} \log(\mu(\mathbf{u}_u^\top \mathbf{v}_i - \mathbf{u}_u^\top \mathbf{v}_j)) \\ &= - \sum_{u \in \mathcal{U}} \sum_{i \in \mathcal{I}, y_{ui}=1} \sum_{j \in \mathcal{I}, y_{uj}=0} \log(\mu(\mathbf{u}_u^\top (\mathbf{v}_i - \mathbf{v}_j))) \\ &= - \frac{1}{2} \sum_{u \in \mathcal{U}} \left(\sum_{i \in \mathcal{I}, y_{ui}=1} \sum_{j \in \mathcal{I}, y_{uj}=0} \log(\mu(\mathbf{u}_u^\top (\mathbf{v}_i - \mathbf{v}_j))) + \sum_{i \in \mathcal{I}, y_{ui}=0} \sum_{j \in \mathcal{I}, y_{uj}=1} \log(\mu(\mathbf{u}_u^\top (\mathbf{v}_j - \mathbf{v}_i))) \right) \\ &= - \frac{1}{2} \sum_{u \in \mathcal{U}} \left(\sum_{(i,j) \in \mathcal{I}', y'_{u,ij}=1} \log(\mu(\mathbf{u}_u^\top \mathbf{v}'_{ij})) + \sum_{(i,j) \in \mathcal{I}', y'_{u,ij}=0} \log(\mu(-\mathbf{u}_u^\top \mathbf{v}'_{ij})) \right) \end{aligned}$$

If the activate function $\mu(\cdot)$ is taken as the Sigmoid function $\sigma(\cdot)$, we have:

$$\begin{aligned} \mathcal{L}_{BPR} &= - \frac{1}{2} \sum_{u \in \mathcal{U}} \left(\sum_{(i,j) \in \mathcal{I}', y'_{u,ij}=1} \log(\sigma(\mathbf{u}_u^\top \mathbf{v}'_{ij})) + \sum_{(i,j) \in \mathcal{I}', y'_{u,ij}=0} \log(1 - \sigma(\mathbf{u}_u^\top \mathbf{v}'_{ij})) \right) \\ &= - \frac{1}{2} \sum_{u \in \mathcal{U}} \sum_{(i,j) \in \mathcal{I}'} (y'_{u,ij} \log(\sigma(\mathbf{u}_u^\top \mathbf{v}'_{ij})) + (1 - y'_{u,ij}) \log(1 - \sigma(\mathbf{u}_u^\top \mathbf{v}'_{ij}))) \end{aligned} \quad (7)$$

From Equation 7, the BPR loss can be reframed as the BCE loss with the hyper-items space \mathcal{I}' . This allows the analyses on point-wise losses to be easily extended to BPR loss.

A.1.2 Suitability of ReSN for BPR Loss

As delineated above, BPR can be regarded as a specialized point-wise loss by introducing the concept of hyper-items. Let's denote the embeddings of these hyper-items with matrix $\mathbf{V}' \in \mathbb{R}^{m^2 \times d}$, where the $(i \cdot m + j)$ -th row corresponds to the embedding of the ij -th hyper-item $\mathbf{v}'_{ij} = \mathbf{v}_i - \mathbf{v}_j$. One might infer that an apt regularizer for the BPR loss would be $\frac{\|\mathbf{U}\mathbf{V}'^\top \mathbf{V}' \mathbf{U}^\top \mathbf{e}\|^2}{\|\mathbf{V}' \mathbf{U}^\top \mathbf{e}\|^2}$, rather than $\frac{\|\mathbf{U}\mathbf{V}^\top \mathbf{V} \mathbf{U}^\top \mathbf{e}\|^2}{\|\mathbf{V} \mathbf{U}^\top \mathbf{e}\|^2}$.

As for the numerator, we have:

$$\begin{aligned} \mathbf{V}'^\top \mathbf{V}' &= \sum_{i,j \in \mathcal{I}} (\mathbf{v}_i - \mathbf{v}_j)^\top (\mathbf{v}_i - \mathbf{v}_j) \\ &= 2m \sum_{i \in \mathcal{I}} \mathbf{v}_i^\top \mathbf{v}_i - 2 \left(\sum_{i \in \mathcal{I}} \mathbf{v}_i \right)^\top \left(\sum_{i \in \mathcal{I}} \mathbf{v}_i \right) = 2m \mathbf{V}^\top \mathbf{V} - 2m^2 \bar{\mathbf{v}}^\top \bar{\mathbf{v}} \end{aligned} \quad (8)$$

where $\bar{\mathbf{v}} = \sum_{i \in \mathcal{I}} \mathbf{v}_i / m$ denote the mean vector of the item embeddings. Furthermore, current literature posits that an ideal item representation should emulate a uniform distribution over the unit ball [53]. This implies that $\bar{\mathbf{v}}$ tends to gravitate towards the origin. Thus, $\mathbf{V}'^\top \mathbf{V}'$ can be approximated by $\mathbf{V}^\top \mathbf{V}$ and $\|\mathbf{U}\mathbf{V}'^\top \mathbf{V}' \mathbf{U}^\top \mathbf{e}\|^2$ can be approximated by $\|\mathbf{U}\mathbf{V}^\top \mathbf{V} \mathbf{U}^\top \mathbf{e}\|^2$.

Similarly, for the denominator:

$$\begin{aligned}
\|\mathbf{V}'\mathbf{U}^\top\mathbf{e}\|^2 &= \sum_{i,j \in I} (\mathbf{v}_i\mathbf{U}^\top\mathbf{e} - \mathbf{v}_j\mathbf{U}^\top\mathbf{e})^\top (\mathbf{v}_i\mathbf{U}^\top\mathbf{e} - \mathbf{v}_j\mathbf{U}^\top\mathbf{e}) \\
&= 2m \sum_{i \in I} (\mathbf{v}_i\mathbf{U}^\top\mathbf{e})^\top (\mathbf{v}_i\mathbf{U}^\top\mathbf{e}) - 2 \left(\sum_{i \in I} \mathbf{v}_i\mathbf{U}^\top\mathbf{e} \right)^\top \left(\sum_{i \in I} \mathbf{v}_i\mathbf{U}^\top\mathbf{e} \right) \\
&= 2m(\mathbf{V}\mathbf{U}^\top\mathbf{e})^\top (\mathbf{V}\mathbf{U}^\top\mathbf{e}) - 2m^2(\bar{\mathbf{v}}\mathbf{U}^\top\mathbf{e})^\top (\bar{\mathbf{v}}\mathbf{U}^\top\mathbf{e})
\end{aligned} \tag{9}$$

We can deduce $\|\mathbf{V}'\mathbf{U}^\top\mathbf{e}\|^2$ can be approximated by $\|\mathbf{V}\mathbf{U}^\top\mathbf{e}\|^2$. Consequently, ReSN emerges as a logical regularizer even for the BPR loss. This assertion is also validated by our experiments.

A.2 Proof of Theorem 1

The proof procedure of Theorem 1 consists of four parts:

- 1) we first showcase the relations between \mathbf{Y} with $\hat{\mathbf{Y}}$ under the condition in Theorem 1 and transform $\cos(\mathbf{r}, \mathbf{q}_1)$ into $\cos(\mathbf{r}, \hat{\mathbf{q}}_1)$;
- 2) We then derive the preliminary lower bound of the $\cos(\mathbf{r}, \hat{\mathbf{q}}_1)$ as $\cos(\mathbf{r}, \hat{\mathbf{q}}_1) \geq \frac{\hat{\sigma}_1 \mathbf{e}^\top \hat{\mathbf{p}}_1}{r_{\max} \sqrt{\zeta(2\alpha)}}$;
- 3) We further utilize the property of \mathbf{Y} to give the lower bound of $\mathbf{e}^\top \hat{\mathbf{p}}_1$ as $\mathbf{e}^\top \hat{\mathbf{p}}_1 \geq \hat{\sigma}_1 \sqrt{1 - \frac{r_{\max}(\zeta(\alpha)-1)}{\hat{\sigma}_1^2}}$;
- 4) Finally, we demonstrate $\hat{\sigma}_1^2 \geq r_{\max}$, and give $\cos(\mathbf{r}, \mathbf{q}_1) = \cos(\mathbf{r}, \hat{\mathbf{q}}_1) \geq \sqrt{\frac{2-\zeta(\alpha)}{\zeta(2\alpha)}}$ when $\alpha > 2$.

Part 1: the spectral relation between \mathbf{Y} and $\hat{\mathbf{Y}}$. Here we focus on an embedding-based model with sufficient capacity and optimize it with MSE loss¹: $L_R = \|\mathbf{Y} - \hat{\mathbf{Y}}\|_F^2$. For other losses, like BCE loss, which can be approximated to MSE Loss via Taylor expansion [35]. Based on the theorem of PCA (Principal Component Analysis) [2], the optimal $\hat{\mathbf{Y}}$ will have the same spectrum as the principal dimensions of \mathbf{Y} . That is, their principal dimensional singular value and vector match up. Because of this relation, when analyzing the principle spectral property of $\hat{\mathbf{Y}}$, we can instead shift our focus and look at \mathbf{Y} , making our job easier.

Part 2: preliminary bound of $\cos(\mathbf{r}, \mathbf{q}_1)$. Note that \mathbf{r} can be written as $\mathbf{r} = \mathbf{Y}^\top \mathbf{e}$, where \mathbf{e} denotes the n -dimension vector filled with ones, and \mathbf{Y} can be written as:

$$\mathbf{Y} = \dot{\mathbf{P}}\dot{\Sigma}\dot{\mathbf{Q}}^\top = \sum_{k=1}^L \dot{\sigma}_k \dot{\mathbf{p}}_k \dot{\mathbf{q}}_k^\top \tag{10}$$

through SVD decomposition. We have:

$$\cos(\mathbf{r}, \hat{\mathbf{q}}_1) = \frac{\mathbf{e}^\top \mathbf{Y} \hat{\mathbf{q}}_1}{\|\mathbf{r}\|} = \frac{\mathbf{e}^\top \sum_{k=1}^L \dot{\sigma}_k \dot{\mathbf{p}}_k \dot{\mathbf{q}}_k^\top \hat{\mathbf{q}}_1}{\|\mathbf{r}\|} = \frac{\hat{\sigma}_1 \mathbf{e}^\top \hat{\mathbf{p}}_1}{\|\mathbf{r}\|} \tag{11}$$

where the last equation holds due to the orthogonal of different singular vectors. Further, considering the power-law nature of item popularity, we have:

$$\|\mathbf{r}\| = \sqrt{\sum_{i=1}^m r_i^2} = r_{\max} \sqrt{\sum_{i=1}^m i^{-2\alpha}} \leq r_{\max} \sqrt{\zeta(2\alpha)} \tag{12}$$

By combining the above two formulas, we have:

$$\cos(\mathbf{r}, \hat{\mathbf{q}}_1) \geq \frac{\sigma_1 \mathbf{e}^\top \hat{\mathbf{p}}_1}{r_{\max} \sqrt{\zeta(2\alpha)}} \tag{13}$$

¹In practice, we may introduce weight decay or negative sampling for acceleration or mitigating overfitting. But they are not our focus here we simply take the original loss for theoretical analyses.

Part 3: bound of $\mathbf{e}^\top \hat{\mathbf{p}}_1$. We first demonstrate that for the matrix \mathbf{Y} , we can always find a non-negative principal singular vector $\hat{\mathbf{q}}_1$. Let define matrix $\mathbf{Z} = \mathbf{Y}^\top \mathbf{Y}$. We can find each element in z_{kl} is non-negative. Note that:

$$\dot{\sigma}_1^2 = \max_{\|\hat{\mathbf{q}}\|=1} \hat{\mathbf{q}}^\top \mathbf{Y}^\top \mathbf{Y} \hat{\mathbf{q}} = \max_{\|\hat{\mathbf{q}}\|=1} \sum_{k=1}^m \sum_{l=1}^m \dot{q}_k z_{kl} \dot{q}_l \quad (14)$$

Suppose we have a principal singular vector \mathbf{q}' with negative elements. Let positions of these negative elements be a set $S = \{k | \mathbf{q}'_k < 0\}$. We always can construct a new m -dimensional vector \mathbf{h} whose k -th element be q'_k if $k \in S$, be $-q'_k$ otherwise. we can find \mathbf{h} would be non-negative and have:

$$\sum_{k=1}^m \sum_{l=1}^m h_k z_{kl} h_l \geq \sum_{k=1}^m \sum_{l=1}^m q'_k z_{kl} q'_l = \dot{\sigma}_1^2 \quad (15)$$

Thus, we always have a non-negative principal singular vector \mathbf{h} .

Let l be the ID of the item with the highest popularity. For convenience, here we simply assume $l = 1$. Let \mathbf{y}_k denote the k -th column of matrix \mathbf{Y} . Given the non-negative of $\hat{\mathbf{q}}_1$ and $y_{ui} \in \{0, 1\}$, we have the relation $\mathbf{e}^\top \hat{\mathbf{p}}_1 \geq \mathbf{y}_1^\top \hat{\mathbf{p}}_1$. According to $\mathbf{Y}^\top \hat{\mathbf{p}}_1 = \sigma_1 \hat{\mathbf{q}}_1$, we further have $\mathbf{y}_1^\top \hat{\mathbf{p}}_1 = \dot{\sigma}_1 \dot{q}_{11}$, where \dot{q}_{1k} denotes the k -th element in $\hat{\mathbf{q}}_1$.

Now we turn to derive the lower bound of \dot{q}_{11} . Define a matrix \mathbf{B} , which is a mirror of \mathbf{Y} except the 1-th column is removed. For any $2 \leq j \leq m$, considering $y_{ui} \in \{0, 1\}$, we have:

$$\sum_{i=2}^m \mathbf{y}_j^\top \mathbf{y}_i \leq \sum_{i=2}^m \mathbf{y}_i^\top \mathbf{y}_i = \sum_{i=2}^m r_i \leq r_{\max}(\zeta(\alpha) - 1) \quad (16)$$

It means the sum of any row of the matrix $\mathbf{B}^\top \mathbf{B}$ is smaller than $r_{\max}(\zeta(\alpha) - 1)$. According to the Perron-Frobenius theorem [43], we have the largest eigenvalue value of $\mathbf{B}^\top \mathbf{B}$ is bounded with: $\lambda_1(\mathbf{B}^\top \mathbf{B}) \leq r_{\max}(\zeta(\alpha) - 1)$. Further, we have:

$$\sum_{i=2}^m (\dot{q}_{1i})^2 = \frac{1}{\dot{\sigma}_1^2} \|\mathbf{B}^\top \hat{\mathbf{p}}_1\|_2^2 \leq \frac{1}{\dot{\sigma}_1^2} \lambda_{\max}(\mathbf{B}^\top \mathbf{B}) \leq \frac{r_{\max}}{\dot{\sigma}_1^2} (\zeta(\alpha) - 1) \quad (17)$$

Considering $\hat{\mathbf{q}}_1$ is the normalization term, we can derive the lower bound of the $\mathbf{e}^\top \hat{\mathbf{p}}_1$ as:

$$\mathbf{e}^\top \hat{\mathbf{p}}_1 \geq \dot{\sigma}_1 \dot{q}_{11} \geq \dot{\sigma}_1 \sqrt{1 - \frac{r_{\max}}{\dot{\sigma}_1^2} (\zeta(\alpha) - 1)} \quad (18)$$

Integrating Eq. (18) into Eq. (13), finally we get the lower bound of the $\cos(\mathbf{r}, \hat{\mathbf{q}}_1)$ as:

$$\cos(\mathbf{r}, \hat{\mathbf{q}}_1) \geq \frac{\dot{\sigma}_1^2}{r_{\max} \sqrt{\zeta(2\alpha)}} \sqrt{1 - \frac{r_{\max}(\zeta(\alpha) - 1)}{\dot{\sigma}_1^2}} \quad (19)$$

Part 4: demonstrating $\dot{\sigma}_1^2 \geq r_{\max}$. Let define a matrix $\mathbf{Z} = \mathbf{Y}^\top \mathbf{Y}$. Let l be the ID of the item with the highest popularity. It is easily to find that the ll -th element in \mathbf{Z} have $z_{ll} = r_{\max}$. Let \mathbf{v} be a one-hot vector whose l -th element is one. we have:

$$r_{\max} = \mathbf{v}^\top \mathbf{Z} \mathbf{v} \leq \max_{\|\hat{\mathbf{q}}\|=1} \hat{\mathbf{q}}^\top \mathbf{Z} \hat{\mathbf{q}} = \dot{\sigma}_1^2 \quad (20)$$

Given $\alpha > 2$, we have $\zeta(\alpha) \leq 2$. Considering $\dot{\sigma}_1^2 \geq r_{\max}$, Eq. (19) can be further bounded with:

$$\cos(\mathbf{r}, \hat{\mathbf{q}}_1) \geq \sqrt{\frac{2 - \zeta(\alpha)}{\zeta(2\alpha)}} \quad (21)$$

Due to the alignment of the principal singular values and vectors of \mathbf{Y} and $\hat{\mathbf{Y}}$, we have:

$$\cos(\mathbf{r}, \mathbf{q}_1) \geq \sqrt{\frac{2 - \zeta(\alpha)}{\zeta(2\alpha)}} \quad (22)$$

A.3 Proof of Theorem 2

Let S be a set of users where the most popular item occupies the top-1 recommendation. Let l be the ID of the most popular item. S can be written as:

$$S = \{u \in \mathcal{U} | \hat{y}_{ul} > \hat{y}_{ui}, \forall i \in \mathcal{I}/l\} \quad (23)$$

The ratio of the most popular item occupying top-1 recommendation can be written as $\eta = |S|/n$. We then do some transformation of the condition:

$$\begin{aligned} & \hat{y}_{ul} > \hat{y}_{ui}, \forall i \in \mathcal{I}/l \\ \Leftrightarrow & \sum_{k=1}^L \sigma_k p_{ku} q_{kl} > \sum_{k=1}^L \sigma_k p_{ku} q_{ki}, \forall i \in \mathcal{I}/l \\ \Leftrightarrow & \sigma_1 p_{1u} (q_{1l} - q_{1i}) > \sum_{k=2}^L \sigma_k p_{ku} (q_{ki} - q_{kl}), \forall i \in \mathcal{I}/l \end{aligned} \quad (24)$$

Given the alignment of \mathbf{r} and \mathbf{q}_1 , and the pow-law distribution of the popularity, for any item $i \in \mathcal{I}/l$, the l.h.s of Eq. (24) can be bounded by:

$$\sigma_1 p_{1u} (q_{1l} - q_{1i}) = \sigma_1 p_{1u} \frac{r_l - r_i}{\|\mathbf{r}\|} \geq \sigma_1 p_{1u} \frac{1 - 2^{-\alpha}}{\sqrt{\zeta(2\alpha)}} \quad (25)$$

Besides, given the normalization of the singular vectors, for any item $i \in \mathcal{I}/l$, we can bound the r.h.s of Eq. (24) as:

$$\sum_{k=2}^L \sigma_k p_{ku} (q_{ki} - q_{kl}) \leq \sum_{k=2}^L \sqrt{2} \sigma_k \quad (26)$$

due to the fact that $p_{ku} \leq 1$ and:

$$(q_{ki} - q_{kl})^2 = q_{ki}^2 + q_{kl}^2 - 2q_{ki}q_{kl} \leq 2(q_{ki}^2 + q_{kl}^2) \leq 2 \quad (27)$$

Thus, the condition $y_{ul} > y_{ui}, \forall i \in \mathcal{I}/l$ holds if the following inequality holds:

$$\sigma_1 p_{1u} \frac{1 - 2^{-\alpha}}{\sqrt{\zeta(2\alpha)}} > \sum_{k=2}^L \sqrt{2} \sigma_k \quad (28)$$

It means that we have the lower bound of the η as:

$$\begin{aligned} \eta &= \frac{1}{n} |\{u \in U | y_{ul} > y_{ui}, \forall i \in \mathcal{I}/l\}| \\ &\geq \frac{1}{n} |\{u \in U | \sigma_1 p_{1u} \frac{1 - 2^{-\alpha}}{\sqrt{\zeta(2\alpha)}} > \sum_{k=2}^L \sqrt{2} \sigma_k\}| \\ &= \frac{1}{n} |\{u \in U | p_{1u} > \frac{\sqrt{2\zeta(2\alpha)}}{1 - 2^{-\alpha}} (\frac{\sum_{k=1}^L \sigma_k}{\sigma_1} - 1)\}| \\ &= \frac{1}{n} \phi\left(\frac{\sqrt{2\zeta(2\alpha)}}{1 - 2^{-\alpha}} \left(\frac{\sum_{k=1}^L \sigma_k}{\sigma_1} - 1\right)\right) \end{aligned} \quad (29)$$

where $\phi(a) = \sum_{u \in U} \mathbf{I}[p_{1u} > a]$ is an inverse cumulative function calculating the number of elements p_{1u} in the left principal singular vector \mathbf{p}_1 exceeding a given value a , and the function $\mathbf{I}[\cdot]$ signifies an indicator function.

A.4 Theoretical Analysis on Dimension Collapse via Gradient Optimization

Here we begin by invoking the gradient dynamic theorem from [15, 48, 6] to elucidate the dimension collapse phenomenon and then develop a theorem to illustrate how the singular values impact the popularity bias in recommendations.

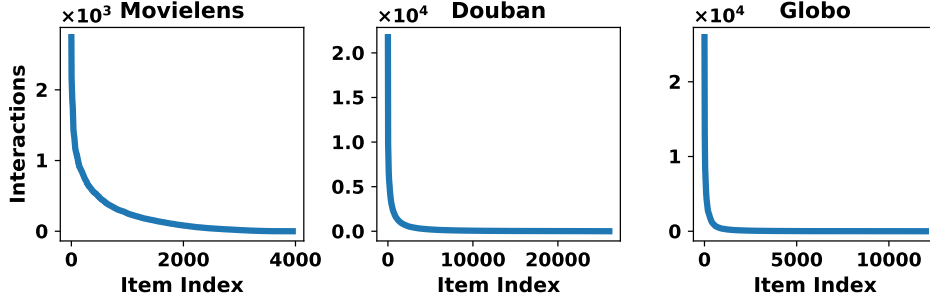


Figure 7: Long-tailed distribution of item popularity in recommendation datasets.

Table 4: The proportion of interactions of the top 20% of popular items in the total number of interactions.

	Movielens-1M	Douban	Globo
%	67.3	86.3	90.5

Theorem 3 (Trajectory of singular values (Eq. (6) in [48])). *When training an MF model via gradient flow (gradient descent with infinitesimally small learning rate), i.e., $\frac{d}{dt}\mathbf{U}(t) = -\frac{dL}{d\mathbf{U}}$, $\frac{d}{dt}\mathbf{V}(t) = -\frac{dL}{d\mathbf{V}}$, the trajectory of singular values during the learning process obeys:*

$$\sigma_k(t) = \frac{s_k e^{2s_k t}}{e^{2s_k t} - 1 + s_k / \sigma_k(0)} \quad (30)$$

where s_k signifies the terminal value of the k -th singular value, i.e., $\sigma_k(t) \rightarrow s_k$ as $t \rightarrow \infty$.

This theorem illustrates a sigmoidal trajectory that begins at some initial value $\sigma_k(0)$ at time $t = 0$ and rises to s_k . The growing trajectory of singular values depends on their respective convergence values. It is coincident with the phenomenon presented in Figure 2(c) — i.e., larger singular values are prioritized. Those small singular values require much more time to reach optimum, easily resulting in dimension collapse.

B Additional Experiments

B.1 Long-tailed Distribution and Bias Amplification in Recommendations

Figure 7 shows the distribution of item popularity (the number of interactions of an item) in the three benchmark datasets. It presents a significant long-tail distribution: a small portion of popular items at the head have a high number of interactions, while the majority of items in the tail have very few interactions. Table 4 shows the proportion of interactions of the top 20% popular items to all interactions. In all three datasets, the interactions of the top 20% popular items accounted for over 60% of all interactions, and in the Globo dataset, it even exceeded 90%.

Figure 8 shows the popularity bias amplification effect in the three benchmark datasets. In all three datasets, a mere 3% of the most popular items accounting for 20% of total interactions occupy over 40% recommendation slots, and in Douban dataset, it even reaches 60%. The disparity in the proportion of interactions to recommendation results effectively demonstrate the amplification effect of popularity bias.

B.2 Comparison between σ_1^2 and r_{max}

Table 5 presents the values of σ_1^2 and r_{max} on three benchmark datasets and different backbone models. It can be observed that in multiple actual datasets, σ_1^2 is significantly larger than r_{max} , exceeding 100 times and more. Combining the bounds given by Eq.(1), $\cos(\mathbf{r}, \mathbf{q}_1) \geq$

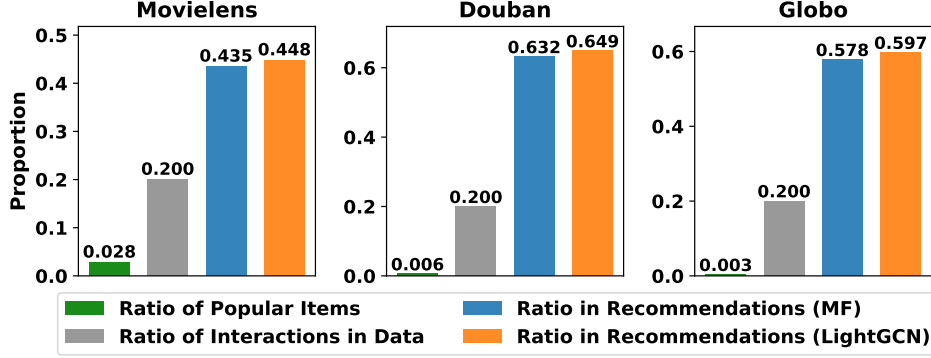


Figure 8: Illustration of popular bias amplification: We divide items into five groups according to their popularity as recent work [68], and focus on the most popular group. The chart displays four bars, representing the ratio of the items in the most popular group, the percentage of interactions originating from these items in the training set, and the percentages of these items appearing in recommendations from MF and LightGCN, respectively.

Table 5: The value of σ_1^2 and r_{max} in different datasets and recommendation models.

Model	MovieLens		Douban		Globo	
	σ_1^2	r_{max}	σ_1^2	r_{max}	σ_1^2	r_{max}
MF	5.6×10^5	4.6×10^3	1.2×10^7	4.7×10^4	8.3×10^6	5.0×10^4
LightGCN	5.7×10^5	4.6×10^3	1.2×10^7	4.9×10^4	8.4×10^6	5.1×10^4

$\frac{\sigma_1^2}{r_{max} \sqrt{\zeta(2\alpha)}} \sqrt{1 - \frac{r_{max}(\zeta(\alpha)-1)}{\sigma_1^2}}$, even if the data is not markedly skewed, *i.e.*, α is not very large and $\zeta(\alpha)$ is not very close to 1, there is still a significant similarity between item popularity vector \mathbf{r} and the principal singular vector \mathbf{q}_1 due to the considerable ratio between σ_1^2 and r_{max} . This observation also helps to explain the prevalence of popularity bias memorization effect in recommendation models and datasets.

B.3 Validation on Approximation

We computed the ideal value of $\|\mathbf{UV}^\top\|_2^2$, as well as the estimated $\frac{\|\mathbf{UV}^\top \mathbf{VU}^\top \mathbf{e}\|^2}{\|\mathbf{UV}^\top \mathbf{e}\|^2}$ from ReSN. Here we well-training the MF model with two losses on three datasets. The results are shown in the Table 6. According to the table, we found that the actual spectral norms and our approximate estimates are very close across diverse losses and datasets. This indicates that the singular vector $\tilde{\mathbf{q}}_1$ obtained through $\frac{\mathbf{UV}^\top \mathbf{e}}{\|\mathbf{UV}^\top \mathbf{e}\|}$, serves as an accurate surrogate for the true value of \mathbf{q}_1 . Therefore, the estimated regularization term is a accurate surrogate for the spectral norm $\|\mathbf{UV}^\top\|_2^2$ which validates the accuracy and rationality of the proposed method.

B.4 Performance with Diverse Embedding sizes

To further evaluate the performance of ReSN, we explored the performance of the model under different embedding dimensions, as shown in Figure 9. It can be seen that, with the increase of embedding dimensions, the performance of all models gradually improves, and our ReSN can outperform the comparison methods under all different embedding dimensions. This further validates the effectiveness of ReSN in terms of performance.

Table 6: Comparison between the actual spectral norm and the estimated approximation.

Datasets	MSE		BCE	
	$\ \mathbf{UV}^\top\ _2^2$	$\ \mathbf{U}(\mathbf{V}^\top \tilde{\mathbf{q}}_1)\ ^2$	$\ \mathbf{UV}^\top\ _2^2$	$\ \mathbf{U}(\mathbf{V}^\top \tilde{\mathbf{q}}_1)\ ^2$
Movielens-1M	5.627×10^5	5.613×10^5	5.629×10^5	5.620×10^5
Douban	1.160×10^7	1.155×10^7	1.161×10^7	1.157×10^7
Globo	8.321×10^6	8.309×10^6	8.327×10^6	8.316×10^6

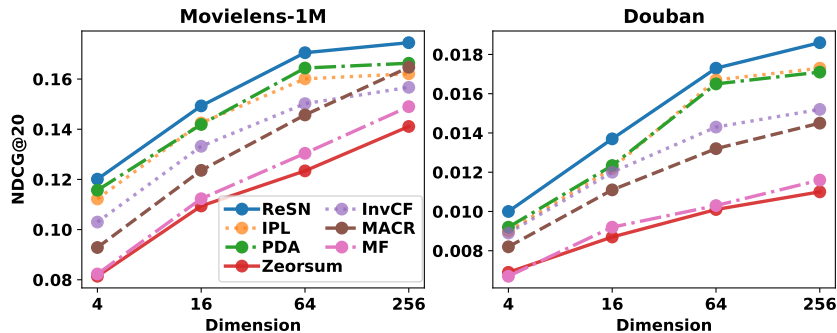


Figure 9: Performance comparison across different embedding dimensions in the Movielens and Douban datasets.

B.5 Efficiency Study

To further validate the effectiveness of our acceleration strategy, we test the running time per epoch of ReSN and the original brute-force strategy employed to compute the gradient of the spectral norm. Also, we present the baseline MF for comparison. The results are presented in Table 7. As can be seen, our acceleration strategy achieves over 3500 and 27000 times impressive speed-up in both datasets, respectively. Moreover, compared with MF, our ReSN does not incur much computational overhead.

C Experimental Settings

C.1 Datasets

We adopt seven real-world datasets to evaluate our model:

- **Movielens-1M** [63]: Movielens is the widely used dataset from [63] and is collected from MovieLens². We use the version of 1M. We transform explicit data into implicit feedback by treating all user-item ratings as positive interactions.
- **Douban** [50]: This dataset is collected from a popular review website Douban³ in China. We transform explicit data into implicit using the same method as applied in Movielens.
- **Globo** [20]: This dataset is a popular dataset collected from the news recommendation website Globo.com⁴.
- **Yelp2018** [27] & **Gowalla** [26]: Gowalla is the check-in dataset obtained from Gowalla and Yelp2018 is from the 2018 edition of the Yelp challenge, containing Yelp’s business reviews and user data. For a fair comparison, these two datasets are used exactly the same as [27] used.

²<https://movielens.org/>

³<https://www.douban.com/>

⁴<http://g1.globo.com/>

Table 7: Running time comparison (s / Epoch).

	Movielens	Douban
MF	0.177	2.098
ReSN	0.181	2.124
ReSN-Direct	649	59239
Speedup Ratio	3585	27890

Table 8: Dataset statistics.

Dataset	#Users	#Items	#Interactions	Sparsity
Movielens-1M	6,022	3,043	995,154	5.431%
Douban	47,890	26,047	7,174,218	0.575%
Globo	160,377	13,096	2,024,510	0.096%
Gowalla	29,858	40,981	1,027,370	0.084%
Yelp2018	31,831	40,841	1,666,869	0.128%
Yahoo!R3	14,382	1,000	129,748	0.902%
Coat	290	295	2776	3.24%

- **Yahoo!R3** [38] & **Coat** [49]: These two datasets are obtained from the Yahoo music and Coat shopping recommendation service, respectively. Both datasets contain a training set of biased rating data collected from normal user interactions and a test set of unbiased rating data containing user ratings on randomly selected items. The rating data are translated to implicit feedback, *i.e.*, interactions with ratings larger than 3 are regarded as positive samples.

Following the standard 10-core setting, we filter out users and items with less than 10 interactions, and we report the statistics of the above datasets after standardization in Table 8.

C.2 Implementation Details

We implement ReSN in Tensorflow [1] and the initialization is unified with Xavier [24]. We optimize all models with Adam [31]. A grid search is conducted to confirm the optimal parameter setting for each model. To be more specific, learning rate is searched in $\{1e^{-2}, 1e^{-3}, 2e^{-4}\}$, weight decay in $\{1e^{-7}, 1e^{-6}, 1e^{-5}, 1e^{-4}, 1e^{-3}\}$. As for the backbone of LightGCN, we utilize three layers of graph convolution network to obtain the best results, with or without using dropout to prevent over-fitting. For ReSN, the coefficient of regularizer β is tuned in the range of $\{1e^{-4}, 1e^{-3}, 1e^{-2}, 1e^{-1}, 5e^{-1}, 1.0, 5.0\}$. For compared methods, we closely refer to configurations provided in their respective publications to ensure their optimal performance.

On the experiments of Pareto curve, besides tuning learning rate and weight decay, we also do following hyperparameter tuning: 1) For PDA, we selected the results of tuning the γ and $\tilde{\gamma}$; 2) For MACR, we selected the results of tuning the coefficient c ; 3) For InvCF, since we found that the differences were not significant after tuning α , λ_1 , and λ_2 , we reported in the form of a point; 4) For Zerosum, we adjusted its regularization term coefficient, but its results varied greatly and oscillated, so we only reported its best overall performance as a point. 5) For IPL, we selected the results of tuning the regularization term coefficient λ_f . All experiments are conducted on a server with Intel(R) Xeon(R) Gold 6254 CPUs.

D Notations

We summarize the notations used in this paper as follows: uppercase bold letters represent matrices (*e.g.*, \mathbf{Y}); lowercase bold letters represent vectors (*e.g.*, \mathbf{r}); $\|\cdot\|_2$ to represent the spectral norm of a matrix, *i.e.*, the largest singular value of the matrix; and $\|\cdot\|$ denotes the L2-norm of a vector. Table 9 provides a more detailed enumeration of the notations used in this paper.

Table 9: Notations in this paper.

Notations	Descriptions
u	a user in the user set \mathcal{U}
i	an item in the item set \mathcal{I}
n	the number of users in \mathcal{U}
m	the number of items in \mathcal{I}
y_{ui}	whether user u has interacted with item i
\mathbf{Y}	the observed interaction matrix
r_i	the number of interactions of item i , <i>i.e.</i> , popularity of item i
\mathbf{r}	the vector of the item popularity over all items
$\mathbf{u}_u, \mathbf{v}_i$	embedding vector of user u and item i
\mathbf{U}, \mathbf{V}	embedding matrices for all users and items
$\hat{\mathbf{Y}}$	predicted matrix of all user-item pairs, <i>i.e.</i> , $\hat{\mathbf{Y}} = \mu(\mathbf{UV}^\top)$
$\sigma_k, \mathbf{p}_k, \mathbf{q}_k$	the k -th largest singular value and its corresponding left and right singular vector of $\hat{\mathbf{Y}}$
α	the shape parameter signifying how severity of long-tail of item popularity
$\zeta(\alpha)$	Rieman zeta function, <i>i.e.</i> , $\zeta(\alpha) = \sum_{j=1}^{\infty} \frac{1}{j^\alpha}$
\mathbf{e}	a n -dimension vector filled with ones